Low-Cost Multi-Criterial Design Optimization of Compact Microwave Passives Using Constrained Surrogates and Dimensionality Reduction

Slawomir Koziel[1,2], Anna Pietrenko-Dabrowska[2], and Muath Al-Hasan[3]

[1]Engineering Optimization & Modeling Center, Reykjavik University, 101 Reykjavik, Iceland, koziel@ru.is,

[2]Faculty of Electronics, Telecommunications and Informatics, Gdansk University of Technology, 80-233 Gdansk, Poland, anna.dabrowska@pg.edu.pl

[3]Networks and Communication Engineering Department, Al Ain University, Abu Dhabi, United Arab Emirates, muath.alhasan@aau.ac.ae

Keywords: Microwave design, compact circuits, multi-objective optimization, EM-driven design, surrogate modeling, principal components, dimensionality reduction.

Abstract

Design of contemporary microwave circuits is a challenging task. Typically, it has to take into account several performance requirements and constraints. The design objectives are often conflicting and their simultaneous improvement may not be possible: instead, compromise solutions are to be sought. Representative examples are miniaturized microwave passives where reduction of the circuit size has a detrimental effect on electrical characteristics. Acquiring information about the best possible design trade-offs is invaluable for the designer yet it entails computationally expensive multi-objective optimization (MO). MO is typically conducted using population-based metaheuristic algorithms, the cost of which might be extremely high. If the circuit performance is evaluated using full-wave electromagnetic (EM) analysis, this cost is often prohibitive. A workaround is the employment of fast surrogate models, and a number of surrogate-assisted frameworks have been proposed in the literature. Unfortunately, a construction of reliable surrogates is hindered in higher-dimensional parameter spaces. The recently proposed constrained modeling mitigates this issue to a certain extent by restricting the modeling process to the region containing the Pareto front to be found. This work proposes a novel surrogate-based MO technique that involves constrained modeling and explicit reduction of the surrogate domain dimensionality. The latter is achieved through the spectral analysis of the extreme Pareto-optimal design set obtained by local search routines. Our methodology is validated using a 15-parameter impedance matching transformer with the Pareto set identified at the cost of a few hundred of EM analyses of the circuit. The numerical experiments also demonstrate a significant reduction of the optimization cost as compared to the state-of-the-art surrogate-assisted MO methods.

1. Introduction

Size reduction of circuits and systems is an important aspect of contemporary microwave design [1]-[4]. Miniaturization has become essential for a number of space-limited application areas such as mobile communications [5], internet of things (IoT) [6], sensors [7], bio-medicine [8], wearable and implantable devices [9], or body area networks [10]. A number of techniques have been developed to permit compact realization of microwave passives. Some of these methods include implementation on high-permittivity substrates [11], folding of conventional transmission lines (TLs) [12], multi-layer circuits (e.g., Low Temperature Cofired Ceramic, LTCC technology [13], [14]), as well as utilization of slow-wave phenomenon where the traditional TLs are replaced by the abbreviated components (e.g., compact microwave resonant cells, CMRCs) [15], [16]. The aforementioned techniques typically imply the increase of the circuit complexity and the appearance of electromagnetic (EM) cross-coupling effects, which cannot be accounted for using circuit-theory means, in particular, equivalent network models. Instead, full-wave EM analysis has to be used which tends to be computationally expensive. High cost negatively affects carrying out EM-driven design procedures, primarily parametric optimization [17], and even more so uncertainty quantification (e.g., statistical analysis [18] or tolerance-aware design [19]). A number of methods have been developed over the years to alleviate the cost-related difficulties [20]-[29]. These include surrogate-based optimization methods (e.g., space mapping [20], response correction [21], response feature technology [22]), machine learning techniques [23], [24], adjoint-based local optimizers [25], [26], as well as gradient-based algorithm with sparse sensitivity updates [27]-[29].

Design of high-frequency components requires taking into account several performance figures pertinent to both electrical and field properties (impedance matching, bandwidth, gain, radiation pattern for antenna arrays) as well as geometrical constraints (e.g., the area occupied by the circuit). Thus, it is a multi-objective task with the design goals at least partially

conflicting: improving of any particular objective has—in general—detrimental effects on the remaining parameters. A representative example is miniaturization of planar microwave passives or antennas: reduction of the circuit footprint results in difficulties with obtaining satisfactory impedance matching or bandwidth [30], may lead to frequency misalignment of transmission/matching characteristics in couplers [31], or degrade gain and efficiency of antennas [32]. In fact, any practical design needs to be a compromise (or trade-off) between the relevant design goals.

Multi-objective design is quantitatively different from single-objective endeavors already at the level of comparing solutions, which is most often realized using Pareto dominance relation [33]. For practical reasons, multi-objective tasks are commonly reformulated into single-criterial problems due to the availability of relevant solution methods, mainly well-established numerical algorithms (gradient-based [34], computational intelligence [35], [36], etc.). The said reformulation may be realized using objective aggregation (e.g., weighted sum methods [37], goal attainment approach [38]) or by selecting a primary objective while handling the remaining ones through appropriately defined constraints [39]. If the designer's preferences are clearly stated, the latter approach may be effective. An illustrative example is explicit reduction of the circuit footprint with hard acceptance thresholds assumed for electrical performance parameters [40].

Regardless of possible simplifications, multi-objective optimization (MO) is a proper way of generating comprehensive data on available design trade-offs. This sort of information can be used to assess suitability of a particular structure for a given application or to conclusively compare alternative circuit solutions. Nevertheless, MO is quite challenging, mostly due to the incurred computational costs. Nowadays, the most popular algorithmic approaches are population-based metaheuristics, including genetic and evolutionary algorithms [41], particle swarm optimizers [42], differential evolution [43], harmony search [44], firefly

algorithm [45], and a lot more [46], [47]. Population-based methods are capable of yielding the Pareto set in a single run of the respective algorithm, yet their computational complexity is considerable. In practice, they can be applied whenever the evaluation cost of the structure at hand is low, in particular, if reliable analytical or equivalent network models are available. Direct application of full-wave EM models for MO usually turns prohibitive. A viable alternative is utilization of surrogate modeling techniques in combination with metaheuristics [48]-[50]. Another option are deterministic methods (e.g., point-by-point Pareto front exploration [51], generalized bisection algorithm [52], etc.).

In this work, a novel algorithmic framework for multi-objective optimization of compact microwave passives is proposed. Our methodology is a surrogate-assisted approach that involves the concept of domain confinement [53] but also employs principal component analysis (PCA) [54] for explicit reduction of the parameter space dimensionality. To reduce the computational overhead related to training data acquisition, the surrogate is constructed in the region containing the Pareto front, estimated using a few designs representing single-objective optima (extreme Pareto-optimal points [55]). The surrogate serves as a prediction tool to yield an initial approximation of the Pareto set and to carry out the space-mapping-based refinement process. The presented technique is illustrated using a 15-parameter miniaturized impedance matching transformer with the Pareto set obtained at the cost of a few hundred of EM analyses. Comparative experiments demonstrate advantages of our method over two state-of-the-art surrogate-based benchmark algorithms in terms of computational efficiency.

2. Low-Cost Multi-Objective Optimization of Microwave Components Using Surrogate Models in Confined Domains

The purpose of this section is to formulate the multi-objective optimization (MO) procedure introduced in the paper. In order to put it in a proper context, a general surrogate-assisted MO technique is first outlined in Section 2.1. Section 2.2 discusses the concept of

parameter space restriction, whereas Section 2.3 presents the details pertaining to the surrogate model set up within the reduced-dimensionality region, defined using the spectral analysis of an auxiliary set of extreme Pareto-optimal points. Section 2.4 summarizes the operation of the proposed multi-objective optimization procedure and illustrates it using a flow diagram.

2.1. Multi-Objective Design Using Surrogate Models

We assume N_{obj} design objectives, denoted as F_k, $k = 1, \ldots, N_{obj}$. The aim is to minimize all of them simultaneously. Because the objectives are normally at least partially conflicting, the goal of multi-objective optimization (MO) is to identify a so-called Pareto front which consists of globally non-dominated solutions also referred to as Pareto-optimal points [41]. The relation $\angle$ [56] allows for comparing the vector-valued solutions by stating that the objective vector $\boldsymbol{F}_1 = [F_{1.1} \ldots F_{1.Nobj}]^T$ dominates over the vector $\boldsymbol{F}_2 = [F_{2.1} \ldots F_{2.Nobj}]^T$ (or $\boldsymbol{F}_1 \angle \boldsymbol{F}_2$) if $F_{1.j} \leq F_{2.j}$ for all j and the inequality is strict for at least one j. No elements of the Pareto front are dominated by any other solutions; thus, they are equally good from the MO point of view. In practice, the aim is to identify a discrete representation of the front, referred to as the Pareto set.

The primary model of the microwave component under design is a full-wave electromagnetic (EM) one, denoted as $\boldsymbol{R}(\boldsymbol{x})$, where $\boldsymbol{x}$ stands for a vector of parameters (typically, the geometrical dimensions of the circuit). As discussed in Section 1, direct multi-objective optimization of the EM model entails significant computational expenses. This is a serious practical problem, particularly if the population-based algorithms are employed as the solution approaches of choice. A possible and popular workaround this issue is the application of surrogate modelling methods [48]-[50]. The fast replacement model, here denoted as $\boldsymbol{R}_s$, allows for massive evaluations of the structure at hand, as required by evolutionary or similar methods, at low cost. Most often $\boldsymbol{R}_s$ is constructed as a data-driven surrogate. The widely used methods include kriging interpolation [57], radial-basis functions [58], Gaussian process regression [59], or neural networks [48]. It should be mentioned that several surrogate-based

MO techniques have been proposed recently that do not involve population-based method to generate the Pareto set (e.g., [51], [52]).

A further mitigation of the high cost issue can be achieved by incorporating variable-fidelity simulation models. Perhaps the most straightforward way of implementing lower-fidelity models is to use coarser discretization of the structure under design [60], which can be accompanied by additional simplifications (e.g., the use of perfect metal conductors, neglecting dielectric losses, or reducing the computational domain [60]). This approach leads to additional savings, especially at the stage of acquiring the training data for surrogate model construction. However, it also requires some caution because of unavoidable misalignment between the models of various fidelities. In particular, the Pareto designs rendered by optimizing the low-fidelity-model-based surrogate require additional refinement. This can be realized using a simple response correction (output space mapping, OSM) as proposed in [32]. Given the low-fidelity Pareto-optimal design $\boldsymbol{x}_s^{(k)}$ (one of the designs selected from the initial Pareto set), the refined (high-fidelity) design is obtained as

$$\boldsymbol{x}_f^{(k)} = \arg \min_{\substack{\boldsymbol{x},\, F_2(\boldsymbol{x}) \le F_2(\boldsymbol{x}_s^{(k)}) \\ \vdots \\ F_{N_{obj}}(\boldsymbol{x}) \le F_{N_{obj}}(\boldsymbol{x}_s^{(k)})}} F_1\left(\boldsymbol{R}_s(\boldsymbol{x}) + [\boldsymbol{R}(\boldsymbol{x}_s^{(k)}) - \boldsymbol{R}_s(\boldsymbol{x}_s^{(k)})]\right) \tag{1}$$

The OSM correction term $\boldsymbol{R}(\boldsymbol{x}_s^{(k)}) - \boldsymbol{R}_s(\boldsymbol{x}_s^{(k)})$ is introduced to compensate for the model misalignment and ensures zero-order consistency [61] between $\boldsymbol{R}_s$ and $\boldsymbol{R}$ at $\boldsymbol{x}_s^{(k)}$. The process (1) can be iterated as necessary. It can also be used if the surrogate model is constructed using high-fidelity data because even in this case, the model accuracy is limited due to computational budget constraints related to training data acquisition.

2.2. Parameter Space Reduction Using Single-Objective Optimization Runs

In practice, constructing the surrogate within the entire parameter space is normally impossible due to the curse of dimensionality but also the lack of prior information about the allocation of the Pareto front. On the other hand, the Pareto front typically occupies a small

portion of the space so that it is computationally advantageous to restrict the modelling process to this region. Perhaps the simplest way of estimating such a subset is through the single-objective optima of the form

$$\boldsymbol{x}^{*(k)} = \arg\min_{\boldsymbol{x}} F_k\left(\boldsymbol{R}(\boldsymbol{x})\right) \tag{2}$$

The extreme Pareto-optimal points $\boldsymbol{x}^{*(k)}$ determine the span of the Pareto front and can be used to define a reduced space as the interval $[\boldsymbol{l}^*,\boldsymbol{u}^*]$, where $\boldsymbol{l}^* = \min\{\boldsymbol{x}^{*(1)},\ldots, \boldsymbol{x}^{*(N_{obj})}\}$ and $\boldsymbol{u}^* = \max\{\boldsymbol{x}^{*(1)},\ldots, \boldsymbol{x}^{*(N_{obj})}\}$. The set $[\boldsymbol{l}^*,\boldsymbol{u}^*]$ contains the majority of the Pareto front and it is therefore sufficient to render the surrogate therein. Figure 1 shows the graphical illustration of the parameter space reduction using single-objective optima (2).

2.3. Surrogate Model Domain Definition with Restricted Dimensionality

In pursuit of improving the computational efficiency of the surrogate-assisted multi-objective optimization procedure, an alternative definition of the surrogate model domain is established. While encapsulating a possibly large portion of the Pareto front, it is also featuring reduced dimensionality, which allows for further reduction of the number of training data samples required to set up a reliable replacement model. The very first approximation of the Pareto front allocation can be obtained using the single-objective optimization runs of (2) and the extreme designs $\boldsymbol{x}^{*(k)}$.

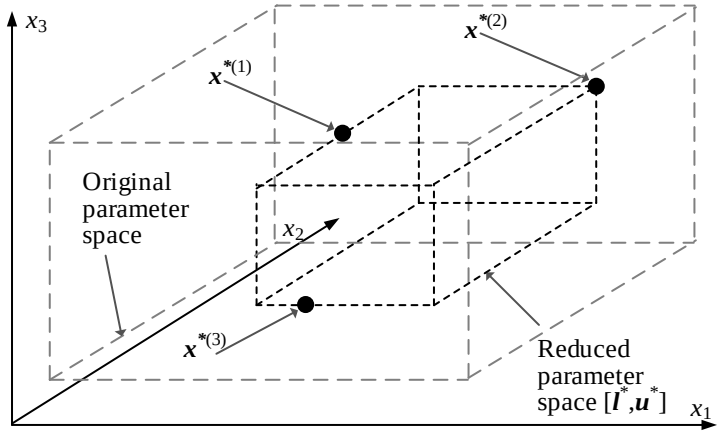

Fig. 1. Graphical illustration of the initial parameter space reduction using extreme Pareto-optimal points $\boldsymbol{x}^{*(k)}$ generated by (2).

A generalized version of the process (2) can be considered that allows for gaining more detailed information about the Pareto front geometry, e.g., its curvature. More specifically, we find the designs minimizing the convex combination of the objectives of the form

$$\boldsymbol{x}^{\boldsymbol{W}} = \arg\min_{\boldsymbol{x}} \sum_{k=1}^{N_{obj}} w_k F_k\left(\boldsymbol{R}(\boldsymbol{x})\right) \tag{3}$$

where $\boldsymbol{W} = [w_1 \ \ldots \ w_{Nobj}]^T$ are the weighting factors such that

$$0 \le w_k \le 1 \quad \text{and} \quad \sum_{k=1}^{N_{obj}} w_k = 1 \tag{4}$$

Setting $\boldsymbol{W} = [0 \ \ldots \ 1 \ \ldots \ 0]^T$ with 1 on the kth position leads to the designs $\boldsymbol{x}^{*(k)}$ obtained using (2). The approximate centre of the front can be found using $\boldsymbol{W} = [1/N_{obj} \ 1/N_{obj} \ \ldots \ 1/N_{obj}]^{\mathrm{T}}$. In general, we denote as $\boldsymbol{x}^{\boldsymbol{w}_k}$, $k = 1, \ldots, p$, the designs produced by (3), (4), to be used in surrogate model domain definition.

The designs $\boldsymbol{x}^{\boldsymbol{w}_k}$ are used to obtain more precise allocation of the Pareto front, both in terms of its span and the most important directions that need to be considered in the optimization process. For that purpose, we consider the covariance matrix of the set $\{\boldsymbol{x}^{\boldsymbol{w}_k}\}$

$$\boldsymbol{C} = \frac{1}{p-1} \sum_{k=1}^{p} (\boldsymbol{x}^{\boldsymbol{w}_k} - \boldsymbol{x}_m)(\boldsymbol{x}^{\boldsymbol{w}_k} - \boldsymbol{x}_m)^T \tag{5}$$

where $\boldsymbol{x}_m = p^{-1} \sum_{k=1,\ldots,p} \boldsymbol{x}^{\boldsymbol{w}_k}$ is the centre of the set $\{\boldsymbol{x}^{\boldsymbol{w}_k}\}$. We also denote by $\{\boldsymbol{v}_k, \lambda_k\}$ $k = 1, \ldots, p - 1$, the eigenvectors (i.e., the principal components) of $\{\boldsymbol{x}^{\boldsymbol{w}_k}\}$ and their corresponding eigenvalues. The eigenvalues quantify the spread (variance) of the designs $\boldsymbol{x}^{\boldsymbol{w}_k}$. They are arranged in a descending order, i.e., $\lambda_1 \ge \lambda_2 \ge \ldots \ge \lambda_{p-1} \ge 0$. Furthermore, we define the matrix $\boldsymbol{V}_K = [\boldsymbol{v}_1 \ \ldots \ \boldsymbol{v}_K]$, with the first k eigenvectors being the columns.

The goal is to define the domain X_S of the surrogate model so that it is spanned by the most important principal components of the set $\{\boldsymbol{x}^{\boldsymbol{w}_k}\}$, i.e., those corresponding to the largest eigenvalues. In practice, as only a few reference points are available, all eigenvectors will be

employed because the number of these is still much smaller than the original dimensionality n of the parameter space.

The technicalities of the domain definition are described below. First, we consider the expansions of the vectors $\boldsymbol{x}^{\boldsymbol{w}_k}$ w.r.t. $\boldsymbol{v}_j$ as

$$\bar{\boldsymbol{x}}^{\boldsymbol{w}_k} = \boldsymbol{x}_m + \sum_{j=1}^{p} b_{kj}\boldsymbol{v}_j \tag{6}$$

The bar on the left-hand-side of (6) is added to indicate that the expansion represents the part of $\boldsymbol{x}^{\boldsymbol{w}_k}$ that belongs to the affine space spanned by $\boldsymbol{x}_m$ and $\boldsymbol{V}$. The expansion coefficients b_{kj} can be found analytically as $b_{kj} = \boldsymbol{v}_j[\boldsymbol{v}_j^T(\boldsymbol{x}^{\boldsymbol{w}_k} - \boldsymbol{x}_m)]$. Some additional notation is also used

$$b_{j.\max} = \max\{k : b_{kj}\}, \quad b_{j.\min} = \min\{k : b_{kj}\} \tag{7}$$

$$b_{j.0} = \frac{b_{j.\min} + b_{j.\max}}{2}, \quad j = 1, \ldots, p \tag{8}$$

$$\boldsymbol{b}_0 = \left[b_{1.0} \ldots b_{p.0} \right]^T \tag{9}$$

$$\boldsymbol{\lambda}_{\boldsymbol{b}} = \left[\lambda_{b1} \ldots \lambda_{bp} \right]^T \tag{10}$$

The entries of vector $\boldsymbol{\lambda}_{\boldsymbol{b}}$ are calculated as $\lambda_{bj} = (b_{j.\max} - b_{j.\min})/2$.

The surrogate model domain is defined as $X_S = X_K$ for the user-selected value of K with

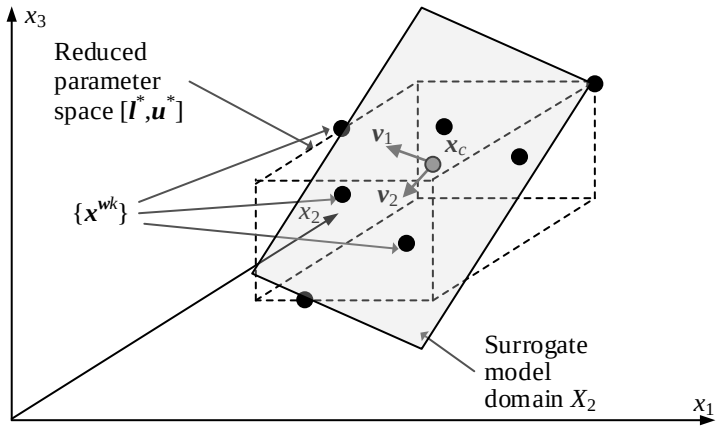

Fig. 2. Definition of the surrogate model domain (here, two-dimensional X_2) using the spectral analysis of the reference set $\{\boldsymbol{x}^{\boldsymbol{w}_k}\}$. In the example shown, the domain is spanned by the two most dominant principal components of $\{\boldsymbol{x}^{\boldsymbol{w}_k}\}$.

$$X_k = \left\{ \begin{array}{c} \boldsymbol{x} = \boldsymbol{x}_c + \sum_{j=1}^{K} (2\lambda_j - 1)\lambda_{b_j} \boldsymbol{a}_j \\ 0 \le \lambda_j \le 1, \quad j = 1, ..., K \end{array} \right\} \tag{11}$$

in which

$$\boldsymbol{x}_c = \boldsymbol{x}_m + \boldsymbol{V}\boldsymbol{b}_0 \tag{12}$$

The set X_K contains all designs $\boldsymbol{x}^{w_k}$ in the directions $\boldsymbol{v}_j$, $j = 1, \ldots, K$. Figure 2 provides a graphical illustration of the concepts pertinent to surrogate model definition.

The surrogate model is constructed in X_S using kriging interpolation [48]. The training samples $\boldsymbol{z} = [z_1 \ \ldots \ z_K]^T$ are first allocated using modified Latin Hypercube Sampling (LHS) [62] in the normalized hypercube $[0\ 1]^K$ (K-times Cartesian product of intervals [0 1]), i.e., $0 \le z_j \le 1$, $j = 1, \ldots, K$. The samples in X_S are obtained using the affine mapping h defined as

$$\boldsymbol{y} = h(\boldsymbol{z}) = \boldsymbol{x}_c + \sum_{j=1}^{K} (2z_j - 1)\lambda_{b_j} \boldsymbol{v}_j \tag{13}$$

In (13), we use the same notation as before: λ_{bj} are the coefficients defined in (10), whereas $\boldsymbol{v}_j$ are the eigenvectors of the covariance matrix $\boldsymbol{C}$ (5).

2.4. Multi-Objective Design Framework with Dimensionality-Reduced Surrogate

The multi-objective optimization framework presented in this work adheres to the overall surrogate-assisted strategy described in Section 2.1. The major difference is the way of constraining the domain of the surrogate model, which is realized as discussed in Section 2.3. Once constructed, the surrogate is employed to generate the initial approximation of the Pareto front using multi-objective evolutionary algorithm (MOEA) [56]. The selected Pareto designs are refined as described in Section 2.1 (cf. (1)). Figure 3 shows the flow diagram of the entire algorithm. It should be noted that although the domain of the surrogate model utilized to render the initial approximation of the Pareto set is a low-dimensional set, it is embedded in the

original design space so that the Pareto-optimal solutions produced by the proposed method already reside in the original space. The assumption is that the information about the front contained along the principal dimensions used to span the domain contain sufficient amount of information about the Pareto front, which is ensured by using a sufficient number of reference designs $\boldsymbol{x}^{wj}$ to account for the front geometry.

At this point, it is necessary to clarify some details concerning surrogate model optimization. Although the model is defined over $X_S = X_K$, it is more convenient to formally conduct the optimization process in the normalized domain $[0\ 1]^K$. For the purpose of evaluating the design objectives, one uses the mapping $h : [0,1]^K \rightarrow X_S$ (cf. (13)), so that we have $F_k(\boldsymbol{R}(\boldsymbol{x})) = F_k(\boldsymbol{R}(h(\boldsymbol{z})))$ with $\boldsymbol{z} \in [0\ 1]^K$.

3. Demonstration Case Study and Benchmarking

The presented MO algorithm is demonstrated here using an exemplary three-section 50-to-100 ohm impedance matching transformer, optimized for two design objectives: minimization of the in-band reflection and minimization of the circuit footprint area. Our methodology is compared to two state-of-the-art surrogate-assisted optimization frameworks.

3.1. Impedance Matching Transformer. Circuit Description and Design Objectives

Consider the impedance matching transformer shown in Fig. 4(b) [63], constructed using compact microstrip resonant cells (CMRCs, see Fig. 4(a)). Replacing conventional transmission lines by CMRCs allows for shortening of the structure. The design variables are $\boldsymbol{x} = [l_{1.1}\ l_{1.2}\ w_{1.1}\ w_{1.2}\ w_{1.0}\ l_{2.1}\ l_{2.2}\ w_{2.1}\ w_{2.2}\ w_{2.0}\ l_{3.1}\ l_{3.2}\ w_{3.1}\ w_{3.2}\ w_{3.0}]^T$. The structure is implemented on RF-35 substrate ($\varepsilon_r = 3.5$, $h = 0.762$ mm). The transformer is supposed to operate within the frequency range from 1.75 GHz to 4.25 GHz.

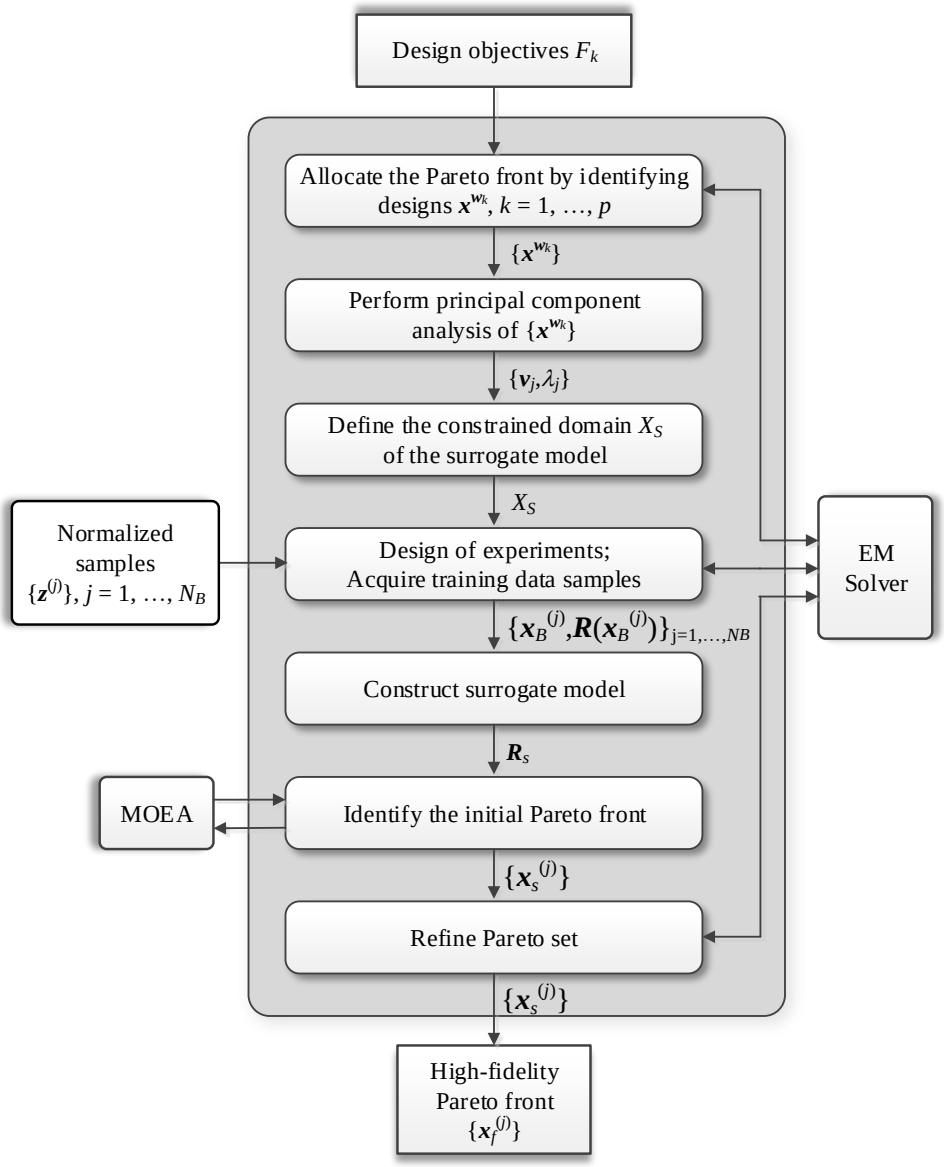

Fig. 3. Multi-objective optimization procedure with dimensionality-reduced surrogate: flow diagram.

In the optimization process, we consider two objectives:

- Minimization of the in-band reflection (F_1);
- Minimization of the footprint area (F_2), defined as the area of the smallest rectangle encapsulating the circuit.

The EM simulation model $\boldsymbol{R}$ is implemented in CST Microwave Studio and evaluated by the transient solver (~280,000 mesh cells, simulation time 2.5 min).

3.2. Optimization Setup and Results

The surrogate model domain is established using the two extreme Pareto-optimal designs $\boldsymbol{x}^{w1} = \boldsymbol{x}^{*(1)}$ = [3.66 0.28 0.77 0.54 0.30 4.32 0.28 0.51 0.24 1.62 4.50 0.20 0.29 0.26 0.57]^T (best reflection design), $\boldsymbol{x}^{w2} = \boldsymbol{x}^{*(2)}$ = [3.54 0.15 0.80 0.16 0.33 2.55 0.15 0.19 0.47 1.42 3.18 0.20 0.21 0.29 1.42]^T (minimum footprint design), and two additional points: $\boldsymbol{x}^{w3}$ = [3.67 0.24 0.78 0.40 0.31 3.78 0.25 0.40 0.32 1.73 4.14 0.16 0.26 0.26 0.73]^T, $\boldsymbol{x}^{w4}$ = [2.50 0.15 0.80 0.32 0.38 2.93 0.18 0.31 0.53 1.73 3.11 0.49 0.20 0.27 1.05]^T. These designs are obtained for the weighting factors [w_1 w_2] of (3), (4) set up as follows: [1 0], [0 1], [2/3 1/3], and [1/3 2/3].

The surrogate model was constructed using only 100 training samples. Its relative RMS error, defined as $\|\boldsymbol{R}(\boldsymbol{x}) - \boldsymbol{R}_S(\boldsymbol{x})\|/\|\boldsymbol{R}(\boldsymbol{x})\|$, averaged over the testing set, is 4.3%. The model domain dimensionality is K = 3, which is the maximum possible number because only four designs $\boldsymbol{x}^{wk}$ are utilized. For the sake of benchmarking, two other surrogates were also constructed:

- The model set up in the interval [$\boldsymbol{l}^*$ $\boldsymbol{u}^*$] with $\boldsymbol{l}^*$ = min{$\boldsymbol{x}^{*(1)}$, $\boldsymbol{x}^{*(2)}$, $\boldsymbol{x}^{*(3)}$, $\boldsymbol{x}^{*(4)}$} and $\boldsymbol{u}^*$ = max{$\boldsymbol{x}^{*(1)}$, $\boldsymbol{x}^{*(2)}$, $\boldsymbol{x}^{*(3)}$, $\boldsymbol{x}^{*(4)}$} (i.e., the initially reduced domain, cf. Section 2.2). The error of this surrogate is 10.4% despite using 1,600 training data samples;
- The model set up using the nested kriging framework [53], the recent performance-driven modeling method. The domain of this surrogate was defined using the same designs $\boldsymbol{x}^{*(k)}$, k = 1, …, 4. The model error is 4.1% when rendered using 200 training samples.

The results of multi-objective optimization using the dimensionality-reduced surrogate have been gathered in Table 1 and 2, as well as Figures 5 and 6. Figure 5 shows the initial Pareto set obtained by optimizing the surrogate using MOEA [56], along with the ten designs selected along the Pareto front before and after their refinement. The geometry parameter values for the refined design can be found in Table 1. Figure 6 illustrates the reflection responses of the transformer at the selected designs from Table 1. Table 2 provides a breakdown of the optimization cost of the optimization process.

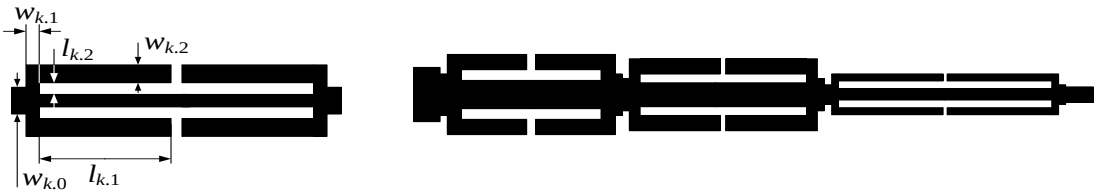

(a) (b)

Fig. 4. Three-section 50-to-100 ohm impedance matching transformer: (a) basic building block of the transformer: compact microstrip resonant cell (CMRC) cell, (b) transformer geometry.

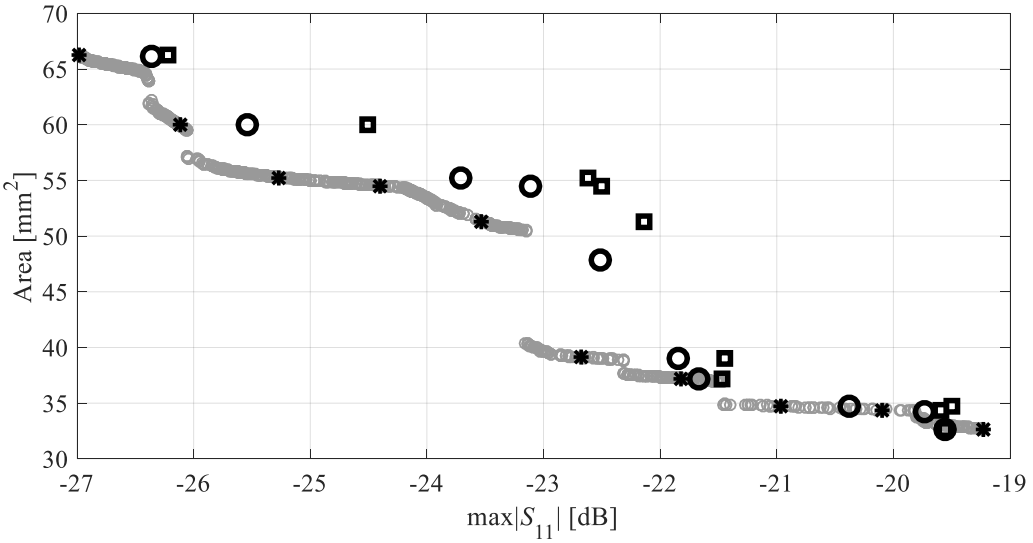

Fig. 5. Three-section impedance matching transformer of Fig. 4(b): (o) initial Pareto set obtained using MOEA, (*) selected designs for refinement, (□) EM-simulated selected designs, (O) EM-simulated refined designs.

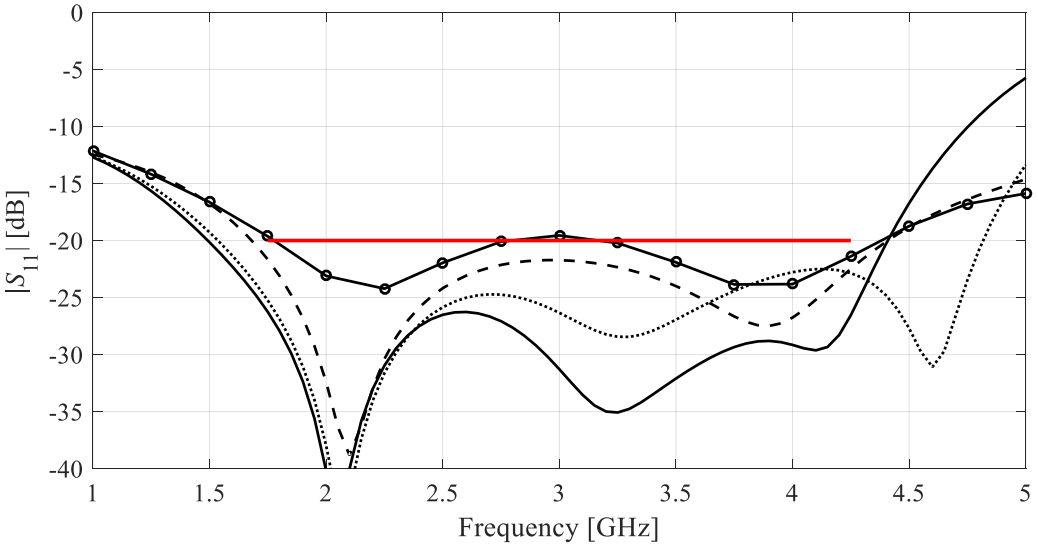

Fig. 6. Three-section impedance matching transformer of Fig. 4(b): reflection characteristics at the selected Pareto-optimal designs of Table 1: $\boldsymbol{x}^{(1)}$ (—), $\boldsymbol{x}^{(4)}$ (····), $\boldsymbol{x}^{(7)}$ (- - -), and $\boldsymbol{x}^{(10)}$ (-o-).

Table 1. Impedance matching transformer: refined Pareto-optimal designs

		Pareto-optimal design									
		$\boldsymbol{x}^{(1)}$	$\boldsymbol{x}^{(2)}$	$\boldsymbol{x}^{(3)}$	$\boldsymbol{x}^{(4)}$	$\boldsymbol{x}^{(5)}$	$\boldsymbol{x}^{(6)}$	$\boldsymbol{x}^{(7)}$	$\boldsymbol{x}^{(8)}$	$\boldsymbol{x}^{(9)}$	$\boldsymbol{x}^{(10)}$
Objectives	F_1 [dB]	–26.4	–25.6	–23.7	–23.1	–22.5	–21.9	–21.7	–20.4	–19.8	–19.6
	F_2 [mm^2]	66.2	60.0	55.3	54.5	47.9	39.1	37.2	34.7	34.3	32.7
Geometry parameters [mm]	$l_{1.1}$	3.51	3.60	3.50	3.56	3.25	2.54	2.59	3.56	3.56	3.46
	$l_{1.2}$	0.26	0.24	0.23	0.23	0.20	0.15	0.15	0.15	0.15	0.15
	$w_{1.1}$	0.77	0.78	0.78	0.78	0.79	0.80	0.80	0.80	0.80	0.80
	$w_{1.2}$	0.50	0.43	0.40	0.39	0.36	0.30	0.30	0.14	0.14	0.17
	$w_{1.0}$	0.31	0.31	0.32	0.32	0.33	0.38	0.37	0.33	0.33	0.34
	$l_{2.1}$	4.13	3.89	3.69	3.65	3.34	2.90	2.88	2.51	2.52	2.58
	$l_{2.2}$	0.27	0.25	0.24	0.24	0.21	0.18	0.18	0.15	0.15	0.15
	$w_{2.1}$	0.47	0.42	0.39	0.38	0.35	0.30	0.30	0.17	0.18	0.20
	$w_{2.2}$	0.29	0.32	0.35	0.35	0.40	0.54	0.53	0.48	0.48	0.47
	$w_{2.0}$	1.76	1.75	1.73	1.70	1.56	1.80	1.71	1.54	1.52	1.45
	$l_{3.1}$	4.34	4.20	4.02	4.01	3.63	3.12	3.11	3.18	3.18	3.17
	$l_{3.2}$	0.22	0.18	0.21	0.20	0.30	0.47	0.47	0.18	0.18	0.22
	$w_{3.1}$	0.27	0.26	0.25	0.25	0.24	0.20	0.20	0.20	0.20	0.21
	$w_{3.2}$	0.26	0.26	0.27	0.27	0.27	0.27	0.27	0.29	0.29	0.29
	$w_{3.0}$	0.55	0.66	0.76	0.80	1.01	1.02	1.09	1.37	1.38	1.40

Table 2. Impedance matching transformer: optimization cost breakdown and benchmarking

Cost item	Surrogate model domain		
	X_S (this work)	X_S (nested kriging [53])	Hypercube [$\boldsymbol{l}^*$,$\boldsymbol{u}^*$]
Extreme points	515 × $\boldsymbol{R}$	515 × $\boldsymbol{R}$	515 × $\boldsymbol{R}$
Data acquisition for kriging surrogate	100 × $\boldsymbol{R}$	200 × $\boldsymbol{R}$	1600 × $\boldsymbol{R}$
MOEA optimization*	N/A	N/A	N/A
Refinement	30 × $\boldsymbol{R}$	30 × $\boldsymbol{R}$	30 × $\boldsymbol{R}$
Total cost#	645 × $\boldsymbol{R}$ (27 h)	745 × $\boldsymbol{R}$ (31 h)	2145 × $\boldsymbol{R}$ (89 h)

* The cost of MOEA optimization is negligible compared to other stages of the process.
# The total cost is expressed in terms of the equivalent number of EM simulations.

3.3. Discussion

Table 2 includes two benchmark techniques, both surrogate-assisted ones. These are (i) the approach with the surrogate model constructed in the interval [$\boldsymbol{l}^*$ $\boldsymbol{u}^*$] (initially reduced space), and (ii) the method involving the surrogate constructed with the nested kriging framework [53]. For the MO algorithm using the surrogate constructed in the interval [$\boldsymbol{l}^*$ $\boldsymbol{u}^*$] (initially reduced

space), the majority of the CPU expenses come from the training data acquisition. The nested kriging model reduces this cost by the factor of eight (from 1600 to 200 samples), whereas the proposed surrogate provides additional and considerable savings (from 200 to 100 samples) while retaining comparable model accuracy. The overall speedup of the presented method is 70 percent and 13 percent over the considered benchmark techniques. If the cost of acquiring the reference designs is not included (it should be observed that this is a common cost necessary to obtain the initial allocation of the Pareto front regardless of any further action), the speedup is as high as 92 percent and 43 percent.

4. Conclusion

The paper presented a low-cost surrogate-assisted technique for multi-objective optimization of miniaturized microwave components. The keystone of the approach is a surrogate model rendered in a reduced-dimensionality domain defined using a small set of designs, pre-optimized in a single-optimization sense, as well as its spectral analysis. The latter yields the domain-spanning directions that represent the variability of the geometry parameters of the circuit under design along its Pareto front. Limiting the domain dimensionality results in a considerable reduction of the number of training points required to construct a reliable surrogate, and, consequently, lowering the overall cost of the optimization process. This has been demonstrated using a three-section impedance matching transformer described by 15 parameters, with the 10-element Pareto set obtained at the total cost of 645 EM simulations of the structure, with only 130 simulations required by the actual MO process. The speedup with respect to two state-of-the-art procedures surrogate-based algorithms is as high as 13 and 70 percent (concerning the total cost), or 43 and 92 percent (concerning the MO part of the process). The presented methodology may be viewed as an alternative approach to cost-

efficient multi-objective design for higher-dimensional problems where construction of the surrogate model is difficult or even impossible due to the large size of the parameter space.

Acknowledgement

The authors would like to thank Dassault Systemes, France, for making CST Microwave Studio available. This work is partially supported by the Icelandic Centre for Research (RANNIS) Grant 206606051 and by National Science Centre of Poland Grant 2018/31/B/ST7/02369, and by the Abu-Dhabi Department of Education and Knowledge (ADEK) Award for Research Excellence 2019 under Grant AARE19-245.

References

[1] S.N. Artemenko, V.S. Igumnov, A.S. Shlapakovsky, and Y.G. Yushkov, "Compact active S-band microwave compressors for producing rectangular pulses of up to 100 ns," *IEEE Trans. Microwave Theory Techn.*, vol. 67, no. 2, pp. 596-605, 2019.

[2] A. Kumar, "An integrated antenna-mixer for compact microwave sensors," *IEEE Int. Microwave and RF Conf (IMaRC)*, Kolkata, India, 28-30 Nov. 2018.

[3] C. Chang, L. Guo, S.G. Tantawi, Y. Liu, J. Li, C. Chen, and W. Huang, "A new compact high-power microwave phase shifter," *IEEE Trans. Microwave Theory Techn.*, vol. 63, no. 6, pp. 1875-1882, 2015.

[4] S. Yan, F. Zhou, J. Dong, X. Zhang, Y. Ding, S. Gao, and X. Cai, "Ultra-compact linear chirped microwave signal generator," *Int. Topical Meeting on Microwave Photonics (MWP)*, Beijing, China, 23-26 Oct. 2017.

[5] H.A.E. Mohamed, H.B. El-Shaarawy, E.A. Abdallah, and H.M.S. El-Hennawy, "A very compact novel multi-band BPF for recent mobile/satellite communication systems," *Progr Electromagn Research C*, vol. 50, pp. 47-56, 2014.

[6] M. Nosrati, Z. Abbasi, M. Baghelani, S. Bhadra, and M. Daneshmand, "Locally strong-coupled microwave resonator using PEMC boundary for distant sensing applications," *IEEE Trans. Microwave Theory Techn.*, vol. 67, no. 10, pp. 4130-4139, 2019.

[7] H. Hamzah, A. Abduljabar, J. Lees, and A. Porch, "A compact microwave microfluidic sensor using a re-entrant cavity," *Sensors*, vol. 18, no. 2, 2018.

[8] L. Yang, Y.J. Zhou, C. Zhang, X.M. Yang, X. Yang, and C. Tan, "Compact multiband wireless energy harvesting based battery-free body area networks sensor for mobile healthcare," *IEEE J Electromagn RF Microw Medicine Biology*, vol. 2, no. 2, pp. 109-115, 2028.

[9] A.K. Biswas and U. Chakraborty, "A compact wide band textile MIMO antenna with very low mutual coupling for wearable applications," *Int J RF Microw Comput Aided Eng*. vol. 29, e21769, 2019.

[10] M. Mohamed, M. Cheffena, A. Moldsvor, and F.P. Fontan, "Physical statistical channel model for off-body area network," *IEEE Ant. Wireless Propag. Lett*, vol. 16, pp. 1516-1519, 2017.

[11] A. Sarkhel, D. Mitra, and S.R. Bhadra-Chaudhuri, "A compact metamaterial with multi-band negative-index characteristics," *Appl Phys A*, vol. 122, no. 4, p. 471, 2016.

[12] D. Letavin, "Miniature microstrip branch line coupler with folded artificial transmission lines," *Int J Electron Commun*. Vol. 99, pp. 8-13, 2019.

[13] D. Wang, K. Chin, W. Che, Y. Wu, and C. Chang, "Compact 60 GHz low-temperature cofired ceramic filter with quasi-elliptic bandpass response," *IET Microwaves Ant. Propag.*, vol. 10, no. 6, pp. 664-669, 2016.

[14] N. Joseph, J. Varghese, M. Teirikangas, T. Vahera, and H. Jantunen, "Ultra-low-temperature cofired ceramic substrates with low residual carbon for next-generation

microwave applications," *ACS Applied Materials Interfaces*, vol. 11, no. 26, pp. 23798-23807, 2019.

[15] Z.Y. Qian and J.X. Chen, "Compact bandpass filter using CMRC-based dual-behavior resonator," *Int. J. RF Microwave CAE*, vol. 29, e21719, 2019.

[16] S. Chen, M. Guo, K. Xu, P. Zhao, L. Dong, and G. Wang, "A frequency synthesizer based microwave permittivity sensor using CMRC structure, " *IEEE Access*, vol. 6, pp. 8556-8563, 2018.

[17] H.M. Torun and M. Swaminathan, "High-dimensional global optimization method for high-frequency electronic design," *IEEE Trans Microwave Theory Techn*., vol. 67, no. 6, pp. 2128-2142, 2019.

[18] D. Wang, Y. Hu, W. Yue, Y. Zeng, Z. Tu, Y. Cai, W. Wang, Q. Fang Q, and M. Yu, "Broadband and compact polarization beam splitter based on an asymmetrical directional coupler with extra optimizing designs," *Appl Opt*. vol. 58, pp. 8221-8226, 2019.

[19] J. Zhang, C. Zhang, F. Feng, W. Zhang, J. Ma, and Q.J. Zhang, "Polynomial chaos-based approach to yield-driven EM optimization," *IEEE Trans. Microwave Theory Tech.*, vol. 66, no. 7, pp. 3186-3199, 2018.

[20] W. Zhang, F. Feng, V.W.R. Gongal-Reddy, J. Zhang, S. Yan, and Q.J. Zhang, "Space mapping approach to electromagnetic centric multiphysics parametric modeling of microwave components," *IEEE Trans Microwave Theory Techn*., vol. 66, no.7, pp. 3169-3185, 2018.

[21] S. Koziel and L. Leifsson, "Simulation-driven design by knowledge-based response correction techniques," Springer, 2016.

[22] S. Koziel and A. Pietrenko-Dabrowska, "Expedited feature-based quasi-global optimization of multi-band antennas with Jacobian variability tracking," *IEEE Access*, vol. 8, pp. 83907-83915, 2020.

[23] J. Joung, "Machine learning-based antenna selection in wireless communications," *IEEE Comm Lett*. Vol. 20, no. 11, pp. 2241-2244, 2016.

[24] L. Xiao, W. Shao, X. Ding, and B. Wang, "Dynamic adjustment kernel extreme learning machine for microwave component design," *IEEE Trans Microwave Theory Techn*., vol. 66, no. 10, pp. 4452-4461, 2018.

[25] H. Malhi and M.H. Bakr, "Geometry evolution of microwave filters exploiting self-adjoint sensitivity analysis," *Int. Conf. Numerical Electromagn. Multiphysics Mod. Opt. (NEMO)*, Ottawa, Canada, 2015.

[26] S. Koziel, F. Mosler, S. Reitzinger, and P. Thoma, "Robust microwave design optimization using adjoint sensitivity and trust regions," *Int. J. RF and Microwave CAE*, vol. 22, no. 1, pp. 10-19, 2012.

[27] S. Koziel and A. Pietrenko-Dabrowska, "Variable-fidelity simulation models and sparse gradient updates for cost-efficient optimization of compact antenna input characteristics," *Sensors*, vol. 19, no. 8, 2019.

[28] S. Koziel and A. Pietrenko-Dabrowska, "Efficient gradient-based algorithm with numerical derivatives for expedited optimization of multi-parameter miniaturized impedance matching transformers," *Radioengineering*, vol. 28, no. 3, pp. 572-578, 2019.

[29] A. Pietrenko-Dabrowska and S. Koziel, „Computationally-efficient design optimization of antennas by accelerated gradient search with sensitivity and design change monitoring," *IET Microwaves Ant. Prop.*, vol. 14, no. 2, pp. 165-170, 2020.

[30] S. Koziel, "Improved trust-region gradient-search algorithm for accelerated optimization of wideband antenna input characteristics," *Int. J. RF & Microwave CAE*, vol. 29, no. 4, e21567, 2019.

[31] C.-H. Tseng, and H.-J. Chen, "Compact rat-race coupler using shunt-stub-based artificial transmission lines," *IEEE Microwave and Wireless Comp. Lett.*, vol. 18, no. 11, pp. 734-736, Nov. 2008.

[32] S. Koziel and S. Ogurtsov, "Multi-objective design of antennas using variable-fidelity simulations and surrogate models," *IEEE Trans. Antennas Prop.*, vol. 61, no. 12, pp. 5931-5939, 2013.

[33] T. Yilmaz, N. Hasan, R. Zane, and Z. Pantic, "Multi-objective optimization of circular magnetic couplers for wireless power transfer applications," *IEEE Trans Magn.*, vol. 53, no. 8, pp. 1-12, 2017.

[34] J. Nocedal and S.J. Wright, *Numerical optimization*. Springer Series in Operations Research, Springer; 2000.

[35] N. Jin and Y. Rahmat-Samii, "Advances in particle swarm optimization for antenna designs: realnumber, binary, single-objective and multiobjective implementations," *IEEE Trans Ant Prop.*, vol. 55, no. 3, pp. 556-567, 2007.

[36] P. Feliot, J. Bect, and E. Vazquez E, "A Bayesian approach to constrained single- and multi-objective optimization," *J. Global Opt.*, vol. 67, no. 1, pp. 1-37, 2017.

[37] R. Wang, Z. Zhou, H. Ishibuchi, T. Liao, and T. Zhang, "Localized weighted sum method for many-objective optimization," *IEEE Trans. Evol. Opt.*, vol. 22, no. 1, pp. 3-18, 2018.

[38] S.S. Rao, *Engineering Optimization*: *Theory and Practice*. John Wiley & Sons; 2009.

[39] S. Koziel and P. Kurgan, "Compact cell topology selection for size-reduction-oriented design of microstrip rat-race couplers," *Int. J. RF & Microwave CAE*, vol. 28, no. 5, 2018.

[40] D.O. Johanesson and S. Koziel, "Feasible space boundary search for improved optimization-based miniaturization of antenna structures," *IET Microwaves, Ant. Prop.*, vol. 12, no. 8, pp. 1273-1278, 2018.

[41] K. Deb, *Multi-objective optimization using evolutionary algorithms*. Wiley, New York; 2001.

[42] A. Lalbakhsh, M.U. Afzal, K.P. Esselle, and B.A. Zeb, "Multi-objective particle swarm optimization for the realization of a low profile bandpass frequency selective surface," *Int Symp. Ant. Prop. (ISAP)*, Hobart, TAS, pp. 1-4, 2015.

[43] L.M. Zheng, S.X. Zhang, S.Y. Zheng, and Y.M. Pan, "Differential evolution algorithm with two-step subpopulation strategy and its application in microwave circuit designs," *IEEE Trans Industrial Inf*., vol. 12, no. 3, pp. 911-923, 2016.

[44] H.V. Hultmann Ayala, L. dos Santos Coelho, V. Cocco Mariani, M.V. Ferreira da Luz, and J.V. Leite, "Harmony search approach based on Ricker map for multiöobjective transformer design optimization," *IEEE Trans. Magn.*, vol. 51, no. 3, 7202304, 2015.

[45] P. Baumgartner, T. Bauernfeind, O. Bíró, A. Hackl, C. Magele, W. Renhart, and R. Torchio, "Multi-objective optimization of Yagi–Uda antenna applying enhanced firefly algorithm with adaptive cost function," *IEEE Trans Magn*., vol. 54, no. 3, pp. 1-4, 2018.

[46] N. Nedjah and L.M. Mourelle, "Evolutionary multi-objective optimisation: a survey," *Int. J. Bio-Inspired Comput*., vol. 7, no. 1, pp. 1-25, 2015.

[47] Q. Long, C. Wu, T. Huang, and X. Wang, "A genetic algorithm for unconstrained multi-objective optimization," *Swarm Evolut. Comput*., vol. 22, pp. 1-14, 2015.

[48] J. Dong, W. Qin, and M. Wang, "Fast multi-objective optimization of multi-parameter antenna structures based on improved BPNN surrogate model," *IEEE Access*, vol. 7, pp. 77692-77701, 2019.

[49] D.K. Lim, K.P. Yi, S.Y. Jung, H.K. Jung, and J.S. Ro, "Optimal design of an interior permanent magnet synchronous motor by using a new surrogate-assisted multi-objective optimization," *IEEE Trans. Magn.*, vol. 51, no. 11, 8207504, 2015.

[50] A. Anand, L. Leifsson, and S. Koziel, "Design strategies for multi-objective optimization of aerodynamic surfaces," *Eng. Comp.*, vol. 34, no. 5, pp. 1724-1753, 2017.

[51] A. Anand, L. Leifsson, and S. Koziel, "Multi-fidelity aerodynamic design trade-off exploration using point-by-point Pareto set identification," *Aerospace Science and Technology*, vol. 79, pp. 399-412, 2018.

[52] S.D. Unnsteinsson and S. Koziel, "Generalized Pareto ranking bisection for computationally feasible multi-objective antenna optimization," vol. 28, no. 8, *Int. J. RF & Microwave CAE*, 2018.

[53] S. Koziel and A. Pietrenko-Dabrowska, "Performance-based nested surrogate modeling of antenna input characteristics," *IEEE Trans. Ant. Prop.*, vol. 67, no. 5, pp. 2904-2912, 2019.

[54] I.T. Jolliffe, *Principal component analysis*, 2nd ed., Springer, New York, 2002.

[55] S. Koziel and A. Pietrenko-Dabrowska, "Rapid multi-objective optimization of antennas using nested kriging surrogates and single-fidelity EM simulation models," *Eng. Comp.*, vol. 37, no. 4, pp. 1491-1512, 2019.

[56] C.M. Fonseca, "Multiobjective genetic algorithms with application to control engineering problems," PhD thesis, Department of Automatic Control and Systems Engineering, University of Sheffield, Sheffield, UK, 1995.

[57] S. An, S. Yang, and O.A. Mohammed, "A Kriging-assisted light beam search method for multi-objective electromagnetic inverse problems," *IEEE Trans. Magn.*, vol. 54, no. 3, pp. 1-4, 2018.

[58] A.I.J. Forrester and A.J. Keane, "Recent advances in surrogate-based optimization," *Prog. Aerospace Sci.*, vol. 45, pp. 50-79, 2009.

[59] W. Lyu, F. Yang, C. Yan, D. Zhou, and X. Zeng, "Multi-objective Bayesian optimization for analog/RF circuit synthesis," *ACM/ESDA/IEEE Design Autom. Conf.*, 2018.

[60] S. Koziel and S. Ogurtsov, “Antenna design by simulation-driven optimization. Surrogate-based approach,” Springer, 2014.

[61] N.M. Alexandrov and R.M. Lewis, “An overview of first-order model management for engineering optimization,” *Optimization Eng.*, vol. 2, no. 4, pp. 413-430, Dec. 2001.

[62] B. Beachkofski and R. Grandhi, “Improved distributed hypercube sampling,” *American Institute of Aeronautics and Astronautics*, paper AIAA 2002-1274, 2002.

[63] A. Pietrenko-Dabrowska and S. Koziel, “Accelerated multi-objective design of miniaturized microwave components by means of nested kriging surrogates,” *Int. J. RF & Microwave CAE*, 2020.